Dynamic Control of Temperature Distributions in Stacks of Intrinsic Josephson Junctions in $Bi_2Sr_2CaCu_2O_{8+\delta}$ for Intense Terahertz Radiation

M. Tsujimoto,* H. Kambara, Y. Maeda, Y. Yoshioka, Y. Nakagawa, and I. Kakeya

Department of Electronic Science and Engineering, Kyoto University, Nishikyo-ku, Kyoto 615-8510, Japan

(Received 12 September 2014; published 29 October 2014)

We study the universal relationship between the hot-spot size and the intensity of terahertz emission from intrinsic Josephson junctions by dynamically controlling the temperature distributions in mesas of $Bi_2Sr_2CaCu_2O_{8+\delta}$. The uniform current bias leads to a significant increase in local temperature compared to the nonuniform current bias. The thermal response of emission differs between the high- and low-bias regimes. We find a strong positive correlation between the emission intensity and the volume of the superconducting parts in the emitting stack. We identify the remarkable increase in the emission intensity by up to 20% by eliminating the excess Joule heat from the mesa.

DOI: 10.1103/PhysRevApplied.2.044016

I. INTRODUCTION

The terahertz wave with a frequency range of 0.3–10 THz is thought to have a great deal of potential both in research and industry [1]. Since the first demonstration of terahertz emission from intrinsic Josephson junctions [2] (IJJs) in high-transition-temperature superconductor $Bi_2Sr_2CaCu_2O_{8+\delta}$ (Bi-2212) [3], terahertz generation using stacks of IJJs has become a major topic of research, both in terms of experiment [3–23] and theory [24–38]. In the IJJ system, an application of a dc voltage V leads to an ac current and electromagnetic emission at the Josephson frequency in the form [39] $f_J = (2e/h)V/N$, where e is the electric charge, h is Plank's constant, and N is the number of active junctions [12]. The intense emission occurs when f_J matches the cavity conditions: in the case of a long rectangular mesa, the fundamental cavity resonance can be excited at $f_{10}^c = c_0/2nw$, where n is the refractive index of Bi-2212 and w is the width of the mesa [3].

The most intriguing physics of the terahertz emissions is the synchronization among thousands of stacked IJJs with distributed widths due to the trapezoidal cross section of the mesa. This system is an instructive demonstration of the Kuramoto model, in which a large number of nonlinear oscillators synchronize due to weak couplings [32]: a Josephson junction array shunted by an inductance-capacitance-resistance load can spontaneously synchronize to a common frequency despite differences in bare frequencies [40]. We perceive essentially the same phenomena in many physical and biological systems, including relaxation oscillator circuits, networks of neurons, and fireflies that flash in unison [41]. In the IJJ system, mutual synchronization based on hot-spot formation has been identified in a recent mixing experiment [36]. A complete study of increases in local temperature in the emitting stack will lead to a further understanding of the nonlinear phase dynamics of the IJJ system. Meanwhile, the effective prevention of overheating is required to increase the emission intensity and may be essential for designing powerful sources [20].

The steady-state temperature distribution in the Bi-2212 mesa is determined by a delicate balance of local Joule heating [29]. In this work, we dynamically control the temperature distributions by altering the dc current distributions and simultaneously monitor the change in the emission intensity. We use a florescent technique to directly image temperature distributions. We find that we can increase emission intensity considerably by preventing the excessive heating that increases hot-spot size. This finding allows for the construction of powerful sources capable of emitting intense terahertz waves.

II. EXPERIMENTAL SETUP

Single crystals of Bi-2212 grown using a traveling-solvent floating-zone technique are annealed at 650 °C for 12 h. The temperature dependence of the c-axis resistivity $\rho_c(T)$ (not shown here) shows the behavior typical of underdoped crystals with $T_c = 78$ K. A small piece of a cleaved crystal is glued onto a sapphire substrate using epoxy resin. The mesa structure with two silver stripe electrodes depicted in Fig. 1(a) is milled from the crystal surface by photolithography and argon ion milling techniques. Figure 1(b) presents the profile of the mesa structure measured using a stylus profiler. The mesa width is $w = 73$ μm and length $\ell = 400$ μm. The thickness of $t = 1.1$ μm corresponds to $N = 720$. Two stripe electrodes 20 μm apart have widths of 15 μm and thicknesses of 0.1 μm. The emitting sample is installed into the He-flow cryostat. The terahertz emission is detected by a Si-composite bolometer with a 1-THz low-pass filter.

*tsujimoto@sk.kuee.kyoto-u.ac.jp

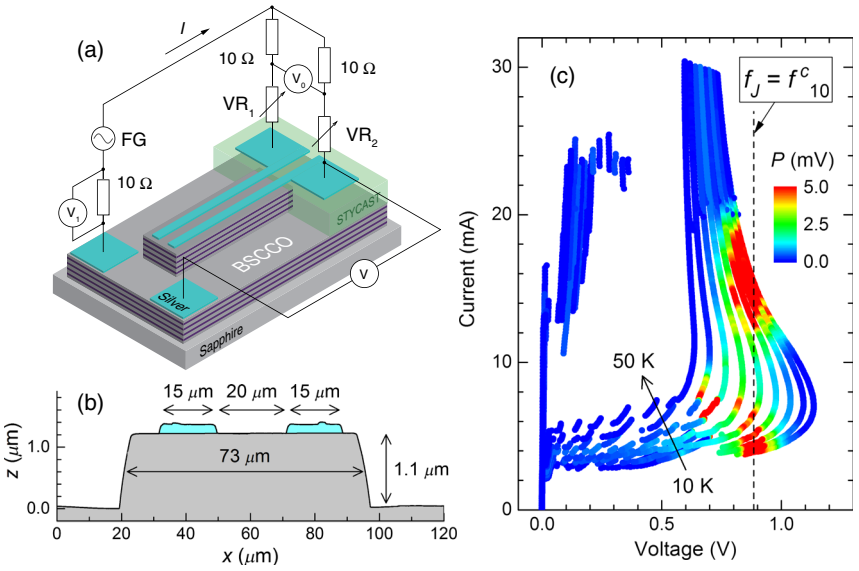

FIG. 1. (a) Schematic view and (b) cross-sectional profile of the Bi-2212 mesa. (c) Four-terminal IVCs in the range of $T_b =$ 10–50 K at 5-K intervals. The color code indicates the bolometer output P. The vertical dashed line represents $f_J = f^c_{10}$.

Figure 1(a) also presents the electrical circuit diagram. Two digital voltmeters V and V_1 are used for measuring voltage V and current I, respectively. We adjust the variable resistors VR_1 and VR_2 in order to alter the ratio of the currents injected via two stripe electrodes. The electrical null method using V_0 enables us to monitor current passing through each electrode. In this paper, we present the results for the following two conditions: nonuniform bias using a left electrode shown in Fig. 1(a) and uniform bias using both electrodes with an equivalent amount of current. Note that in the former case, a left-right reversal produces the same results.

III. RESULTS AND DISCUSSION

Figure 1(c) shows the four-terminal I-V characteristics (IVCs) with color-coded bolometer output P at various bath temperatures T_b. A vertical dashed line at $V = 0.884$ V represents the calculated voltage that satisfies $f_J = f^c_{10}$, where we assume that n has no temperature variation. We indeed observe intense emissions when f_J matches f^c_{10} in two characteristic bias regimes: a high-bias regime ($I =$ 12–20 mA) and a low-bias regime ($I =$ 4–9 mA). We can perceive a gap regime between the two regimes at $I =$ 9–12 mA, where the emission intensities are rather suppressed. This regime suggests the existence of a missing mechanism other than the Josephson and cavity effects in the IJJ stack with distributed widths as an intrinsic disorder. According to an exactly solvable mean-field model for coupled Josephson arrays [40], low-bias emission is reasonably attributable to generic frequency locking, whereas the current condition for high-bias emission has to be modified due to the hot-spot formation. We suppose that extreme temperature inhomogeneity in the mesa is a key ingredient for synchronization in the IJJ stack.

To image the local temperature, we use a fluorescent technique based on the strong temperature dependence of the fluorescence intensity of the coordination complex [42]. A film that consists of europium thenoyltrifluoroacetonate in a polymer matrix of polybutylmethacrylate as the temperature marker is deposited on the surface of the sample by a spin-coating technique and irradiated by 365-nm light emitted by an UV light-emitting diode. A room-temperature CMOS camera with an UV filter is used to acquire the fluorescent image. The acquired data may be directly converted to a surface local temperature $T_{\rm local}$ by calibrating the temperature dependence of the fluorescence intensity. Because the sensitivity of the film depends on the surface materials, i.e., Bi-2212 or silver, a calibration curve must be determined for each surface. Nevertheless, since the inevitable edge effect at the narrow electrode stripes may degrade image quality and obscure details [18], in the present experiment we image $T_{\rm local}$ distributions for only the Bi-2212 surface in order to facilitate the analysis.

Figures 2(a) and 2(b) display the temperature distributions for nonuniform and uniform-bias conditions, respectively. The images are taken with decreasing I from 33 to 9 mA at 6-mA intervals. The orange parts are no longer superconducting with $T_{\rm local} > T_c$. The data for the silver electrodes are not shown here (cf. blacked-out stripes). Note that in the case of nonuniform bias, the current is injected from the lower electrode in Fig. 2(a), as indicated by the red triangle in the upper left. To make a quantitative evaluation of $T_{\rm local}$ in terms of T_c, the temperature profiles along the length (y) of the mesa extracted from Figs. 2(a) and 2(b) are presented in Figs. 2(c) and 2(d), respectively. The temperature profiles along the width (x) are also presented in Figs. 2(e) and 2(f), respectively. Each profile curve is obtained from a smooth fit to the measured data with an uncertainty below 10%.

As shown in Figs. 2(a) and 2(b), the bias uniformity is found to lead to a major difference in $T_{\rm local}$ distributions.

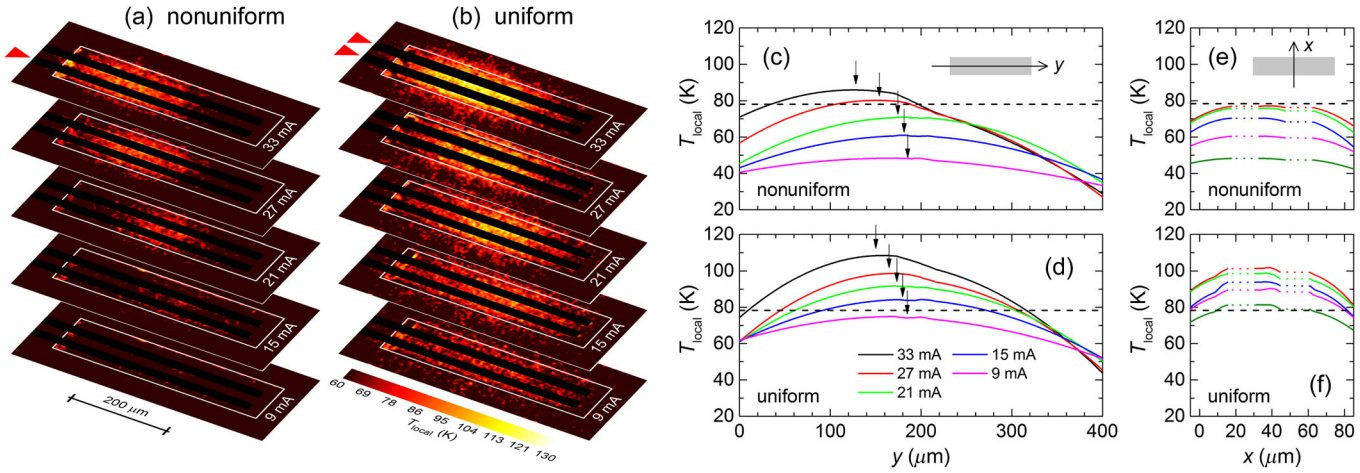

FIG. 2. Temperature distributions in the emitting mesa at $T_b = 4.2$ K for the (a) nonuniform- and (b) uniform-bias cases. The upper triangles mark the electrodes used for the current injection. (c),(d) Temperature profiles along the length of the mesa at $x = w/2$. Arrows indicate the center of the hot spot. (e),(f) Temperature profiles along the width of the mesa at $y = \ell/2$.

First, for nonuniform bias, the hot spot that is initially localized on the left side moves to the center of the mesa as I decreases to 21 mA. The hot spot disappears at 12 mA, resulting in a uniform distribution. Such hot-spot behavior closely correlates with previous observations [4,8,9,23]. In contrast, for uniform bias, although the hot spot moves from the left to the center as I decreases, it has a diameter more than twice that seen in Fig. 2(a). The temperature profiles presented in Fig. 2(d) guide our understanding of the anomalous behavior for the uniform-bias case. As I decreases further, T_{local} over a large area remains higher than T_c, and hot-spot formation lasts until 10 mA. Note that the temperature profiles along x are nearly centrally symmetric even with uniform bias.

From the results of temperature imaging, we presume that emission intensity also has a strong correlation with the volume of the superconducting parts in the emitting mesa. Figure 3(a) shows the IVCs at $T_b = 20$ K for two bias conditions. In the case of uniform bias, the IVC has a contact resistance due to the three-terminal measurement. Figures 3(b) and 3(c) plot $P(V)$ in the high-bias and low-bias regimes, respectively. The blue and red data correspond to nonuniform- and uniform-bias cases, respectively, where V for the latter case has an offset of 0.2 V for ease of comparison. Note that the obtained IVCs are nearly independent of the current conditions except for the contact resistance despite differences in the surface temperature shown in the insets. In the high-bias regime, there is a clear difference in $P(V)$ of 20% between the two cases, whereas in the low-bias regime, $P(V)$ behaves independently of the current conditions. The same behaviors are observed for the whole range of T_b in which emission takes place.

In view of the differences in $P(V)$ combined with the temperature distributions, eliminating excessive heating may prevent the conditions that lead to the loss of superconductivity over the whole mesa, resulting in an increase of the emission intensity. This interpretation is also supported by the fact that increases in P are observable only in the high-bias regime. In addition, low-bias emission seems to be more intense than high-bias emission, suggesting that only the superconducting parts are indeed able to contribute to the emission—nonsuperconducting parts just weaken the emission intensity. We measure three isolated mesas formed on the same base crystal and find that they show reproducible results. The effect is at all significant and universal, and it reveals the new physical finding that the high-bias emission is qualitatively different from the low-bias emission.

We consider a 1D heat-transfer model for the simplest continuous case to explain a major difference in surface

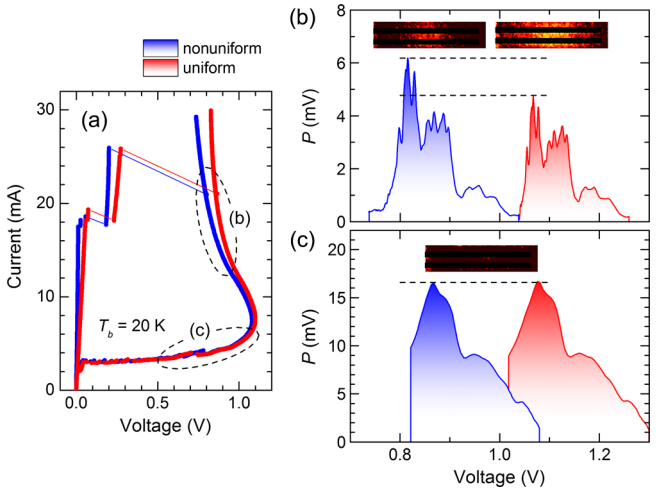

FIG. 3. (a) Four-terminal IVCs at $T_b = 20$ K. $P(V)$ in the high- and low-bias regimes is shown in (b) and (c), respectively, where the blue and red plots indicate the data for nonuniform and uniform bias. V for the latter case has offsets of 0.2 V. The insets beside the data present the corresponding temperature distributions in the mesa.

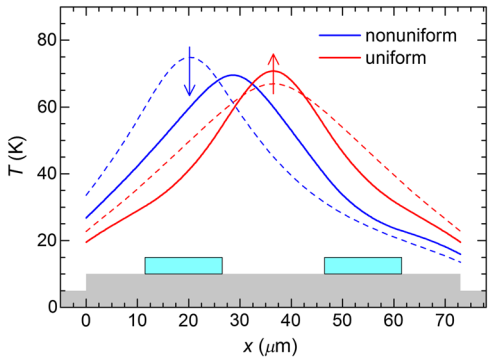

FIG. 4. $T(x)$ profiles calculated by solving Eq. (1) with $I = 21$ mA. Dashed lines represent corresponding results without considering the electrode cooling.

temperature caused by current conditions. In the following simulation, we take into account both Joule heating and conserved cooling at the electrode contacts. The temperature distribution $T(x)$ along the width in thermal equilibrium can be calculated according to the following diffusion equation:

$$-t\frac{d}{dx}\left[\kappa_{ab}(T)\frac{d}{dx}T\right]+\left\{\frac{\kappa_c(T)}{L_1}+\left(\frac{A_2}{A_1}\right)\frac{\kappa_{\mathrm{Ag}}}{L_2}\right\}(T-T_b)=\frac{V^2}{\rho_c(T)t}+i^2(R_cA_1). \quad (1)$$

The second term describes the cooling due to the base crystal and the electrode with the coefficients κ_c/L_1 and κ_{Ag}/L_2, where A_2/A_1 represents the contact area ratio as a reduction factor. The two terms in the right-hand side describe Joule heating due to the c-axis and contact resistances. We use realistic parameters: $L_1 = 20\ \mu$m, $L_2 = 300\ \mu$m, $A_2/A_1 = 2.5\times10^{-3}$, $R_c = 10\ \Omega$, κ_{ab} and κ_c from Ref. [43], and $\kappa_{\mathrm{Ag}} = 1.9\times10^{-4}$ W/mK. The boundary conditions are chosen to be $dT/dx = 0$ (zero flux) at the positions 150 μm apart from both ends of the mesa. The current density at the electrode contacts i is given by I/A_1 for nonuniform bias and by $I/2A_1$ for uniform bias. We numerically solve Eq. (1) using finite element analysis [44]. To find a nontrivial $T(x)$, a proper initial function has to be used. Figure 4 shows calculated $T(x)$ profiles with $I = 21$ mA at $T_b = 4.2$ K. We also plot the calculation results without considering electrode cooling (cf. dashed lines) for comparison. Because we neglect temperature variations along the y and z directions, the calculated T is reasonably lower than the measured $T_{\mathrm{local}}(x)$ at $y = \ell/2$.

Interestingly, for the nonuniform-bias case, a temperature rise at the left contact is shown to be inhibited by the electrode cooling despite stronger heating at the same contact, resulting in lower peak T than that for the uniform-bias case. This is attributed to a larger cooling efficiency determined by $(T - T_b)$. In contrast, the uniform bias leads to higher peak T at the center due to less electrode cooling. This tendency is consistent with observed differences in T_{local} for the two bias cases. Although further studies using a 2D model in order to evaluate temperature variations along the y direction are needed, the present model reveals a substantial difference in T distributions due to both heating and cooling at the electrode contact that have not been studied in previous simulations.

IV. CONCLUSION

In conclusion, we investigate the universal relationship between coherent terahertz-wave emission from mesas of Bi-2212 and temperature distributions by dynamically controlling the temperature distributions. The temperature distributions in emitting mesas are directly imaged using a fluorescent technique. For the high-bias regime, we find that the temperature distributions and the consequent emission intensity vary remarkably depending on the current conditions. This rather surprising phenomenon can be understood by using the simplest 1D model with considering both heating and cooling at the electrode contact. The emission intensity increases by up to 20% with a decrease in the hot-spot size. In contrast to high-bias emission, the low-bias emission intensity remains constant independently of the bias condition consistent with no change in the temperature distribution. Because no regard has been given to the elimination of the excess heat from mesas, further improvements in terms of the sample structure and the bias condition may allow for the construction of powerful and tunable sources that fill a technical gap in the terahertz regime.

ACKNOWLEDGMENTS

The authors thank T. Kashiwagi, H. Minami, and K. Kadowaki for valuable discussions. Comments from H. Asai are greatly appreciated. This work was supported by KAKENHI (Grants No. 23681030, No. 13J04811, and No. 26790032).

[1] M. Tonouchi, Cutting-edge terahertz technology, Nat. Photonics **1**, 97 (2007).
[2] R. Kleiner, F. Steinmeyer, G. Kunkel, and P. Müller, Intrinsic Josephson effects in $Bi_2Sr_2CaCu_2O_8$ single crystals, Phys. Rev. Lett. **68**, 2394 (1992).
[3] L. Ozyuzer, A. E. Koshelev, C. Kurter, N. Gopalsami, Q. Li, M. Tachiki, K. Kadowaki, T. Yamamoto, H. Minami, H. Yamaguchi, T. Tachiki, K. E. Gray, W.-K. Kwok, and U. Welp, Emission of coherent THz radiation from superconductors, Science **318**, 1291 (2007).
[4] H. B. Wang, S. Guénon, J. Yuan, A. Iishi, S. Arisawa, T. Hatano, T. Yamashita, D. Koelle, and R. Kleiner, Hot spots and waves in $Bi_2Sr_2CaCu_2O_8$ intrinsic Josephson junction stacks: A study by low temperature scanning laser microscopy, Phys. Rev. Lett. **102**, 017006 (2009).

[5] H. Minami, I. Kakeya, H. Yamaguchi, T. Yamamoto, and K. Kadowaki, Characteristics of terahertz radiation emitted from the intrinsic Josephson junctions in high-T_c superconductor $Bi_2Sr_2CaCu_2O_{8+\delta}$, Appl. Phys. Lett. **95**, 232511 (2009).

[6] K. Kadowaki, M. Tsujimoto, K. Yamaki, T. Yamamoto, T. Kashiwagi, H. Minami, M. Tachiki, and R. A. Klemm, Evidence for a dual-source mechanism of terahertz radiation from rectangular mesas of single crystalline $Bi_2Sr_2CaCu_2O_{8+\delta}$ intrinsic Josephson junctions, J. Phys. Soc. Jpn. **79**, 023703 (2010).

[7] M. Tsujimoto, K. Yamaki, K. Deguchi, T. Yamamoto, T. Kashiwagi, H. Minami, M. Tachiki, K. Kadowaki, and R. A. Klemm, Geometrical resonance conditions for THz radiation from the intrinsic Josephson junctions in $Bi_2Sr_2CaCu_2O_{8+\delta}$, Phys. Rev. Lett. **105**, 037005 (2010).

[8] H. B. Wang, S. Guénon, B. Gross, J. Yuan, Z. G. Jiang, Y. Y. Zhong, M. Grünzweig, A. Iishi, P. H. Wu, T. Hatano, D. Koelle, and R. Kleiner, Coherent terahertz emission of intrinsic Josephson junction stacks in the hot spot regime, Phys. Rev. Lett. **105**, 057002 (2010).

[9] S. Guénon, M. Grünzweig, B. Gross, J. Yuan, Z. G. Jiang, Y. Y. Zhong, M. Y. Li, A. Iishi, P. H. Wu, T. Hatano, R. G. Mints, E. Goldobin, D. Koelle, H. B. Wang, and R. Kleiner, Interaction of hot spots and terahertz waves in $Bi_2Sr_2CaCu_2O_8$ intrinsic Josephson junction stacks of various geometry, Phys. Rev. B **82**, 214506 (2010).

[10] K. Yamaki, M. Tsujimoto, T. Yamamoto, A. Furukawa, T. Kashiwagi, H. Minami, and K. Kadowaki, High-power terahertz electromagnetic wave emission from high-T_c superconducting $Bi_2Sr_2CaCu_2O_{8+\delta}$ mesa structures, Opt. Express **19**, 3193 (2011).

[11] T. M. Benseman, A. E. Koshelev, K. E. Gray, W.-K. Kwok, U. Welp, K. Kadowaki, M. Tachiki, and T. Yamamoto, Tunable terahertz emission from $Bi_2Sr_2CaCu_2O_{8+\delta}$ mesa devices, Phys. Rev. B **84**, 064523 (2011).

[12] M. Tsujimoto, T. Yamamoto, K. Delfanazari, R. Nakayama, T. Kitamura, M. Sawamura, T. Kashiwagi, H. Minami, M. Tachiki, K. Kadowaki, and R. A. Klemm, Broadly tunable subterahertz emission from internal branches of the current-voltage characteristics of superconducting $Bi_2Sr_2CaCu_2O_{8+\delta}$ single crystals, Phys. Rev. Lett. **108**, 107006 (2012).

[13] I. Kakeya, Y. Omukai, T. Yamamoto, K. Kadowaki, and M. Suzuki, Effect of thermal inhomogeneity for terahertz radiation from intrinsic Josephson junction stacks of $Bi_2Sr_2CaCu_2O_{8+\delta}$, Appl. Phys. Lett. **100**, 242603 (2012).

[14] M. Tsujimoto, H. Minami, K. Delfanazari, M. Sawamura, R. Nakayama, T. Kitamura, T. Yamamoto, T. Kashiwagi, T. Hattori, and K. Kadowaki, Terahertz imaging system using high-T_c superconducting oscillation devices, J. Appl. Phys. **111**, 123111 (2012).

[15] M. Li, J. Yuan, N. Kinev, J. Li, B. Gross, S. Guénon, A. Ishii, K. Hirata, T. Hatano, D. Koelle, R. Kleiner, V. P. Koshelets, H. B. Wang, and P. Wu, Linewidth dependence of coherent terahertz emission from $Bi_2Sr_2CaCu_2O_8$ intrinsic Josephson junction stacks in the hot-spot regime, Phys. Rev. B **86**, 060505(R) (2012).

[16] K. Delfanazari, H. Asai, M. Tsujimoto, T. Kashiwagi, T. Kitamura, T. Yamamoto, M. Sawamura, K. Ishida, C. Watanabe, S. Sekimoto, H. Minami, M. Tachiki, R. A. Klemm, T. Hattori, and K. Kadowaki, Tunable terahertz emission from the intrinsic Josephson junctions in acute isosceles triangular $Bi_2Sr_2CaCu_2O_{8+\delta}$ mesas, Opt. Express **21**, 2171 (2013).

[17] D. Y. An, J. Yuan, N. Kinev, M. Y. Li, Y. Huang, M. Ji, H. Zhang, Z. L. Sun, L. Kang, B. B. Jin, J. Chen, J. Li, B. Gross, A. Ishii, K. Hirata, T. Hatano, V. P. Koshelets, D. Koelle, R. Kleiner, H. B. Wang, W. W. Xu, and P. H. Wu, Terahertz emission and detection both based on high-T_c superconductors: Towards an integrated receiver, Appl. Phys. Lett. **102**, 092601 (2013).

[18] T. M. Benseman, A. E. Koshelev, W.-K. Kwok, U. Welp, V. K. Vlasko-Vlasov, K. Kadowaki, H. Minami, and C. Watanabe, Direct imaging of hot spots in $Bi_2Sr_2CaCu_2O_{8+\delta}$ mesa terahertz sources, J. Appl. Phys. **113**, 133902 (2013).

[19] T. M. Benseman, A. E. Koshelev, W.-K. Kwok, U. Welp, K. Kadowaki, J. R. Cooper, and G. Balakrishnan, The ac Josephson relation and inhomogeneous temperature distributions in large $Bi_2Sr_2CaCu_2O_{8+\delta}$ mesas for THz emission, Supercond. Sci. Technol. **26**, 085016 (2013).

[20] T. M. Benseman, K. E. Gray, A. E. Koshelev, W.-K. Kwok, U. Welp, H. Minami, K. Kadowaki, and T. Yamamoto, Powerful terahertz emission from $Bi_2Sr_2CaCu_2O_{8+\delta}$ mesa arrays, Appl. Phys. Lett. **103**, 022602 (2013).

[21] S. Sekimoto, C. Watanabe, H. Minami, T. Yamamoto, T. Kashiwagi, R. A. Klemm, and K. Kadowaki, Continuous 30 μW terahertz source by a high-T_c superconductor mesa structure, Appl. Phys. Lett. **103**, 182601 (2013).

[22] T. Kashiwagi, K. Nakade, B. Marković, Y. Saiwai, H. Minami, T. Kitamura, C. Watanabe, K. Ishida, S. Sekimoto, K. Asanuma, T. Yasui, Y. Shibano, M. Tsujimoto, T. Yamamoto, J. Mirković, and K. Kadowaki, Reflection type of terahertz imaging system using a high-T_c superconducting oscillator, Appl. Phys. Lett. **104**, 022601 (2014).

[23] H. Minami, C. Watanabe, K. Sato, S. Sekimoto, T. Yamamoto, T. Kashiwagi, R. A. Klemm, and K. Kadowaki, Local SiC photoluminescence evidence of hot spot formation and sub-THz coherent emission from a rectangular $Bi_2Sr_2CaCu_2O_{8+\delta}$ mesa, Phys. Rev. B **89**, 054503 (2014).

[24] A. E. Koshelev and L. N. Bulaevskii, Resonant electromagnetic emission from intrinsic Josephson-junction stacks with laterally modulated Josephson critical current, Phys. Rev. B **77**, 014530 (2008).

[25] S. Lin and X. Hu, Possible dynamic states in inductively coupled intrinsic Josephson junctions of layered high-T_c superconductors, Phys. Rev. Lett. **100**, 247006 (2008).

[26] M. Tachiki, S. Fukuya, and T. Koyama, Mechanism of terahertz electromagnetic wave emission from intrinsic Josephson junctions, Phys. Rev. Lett. **102**, 127002 (2009).

[27] N. Pedersen and S. Madsen, THz generation using fluxon dynamics in high temperature superconductors, IEEE Trans. Appl. Supercond. **19**, 726 (2009).

[28] A. E. Koshelev, Stability of dynamic coherent states in intrinsic Josephson-junction stacks near internal cavity resonance, Phys. Rev. B **82**, 174512 (2010).

[29] A. Yurgens, Temperature distribution in a large $Bi_2Sr_2CaCu_2O_{8+\delta}$ mesa, Phys. Rev. B **83**, 184501 (2011).

[30] V. M. Krasnov, Terahertz electromagnetic radiation from intrinsic Josephson junctions at zero magnetic field via breather-type self-oscillations, Phys. Rev. B **83**, 174517 (2011).

[31] T. Koyama, H. Matsumoto, M. Machida, and Y. Ota, Multi-scale simulation for terahertz wave emission from the intrinsic Josephson junctions, Supercond. Sci. Technol. **24**, 085007 (2011).

[32] S. Lin, X. Hu, and L. Bulaevskii, Synchronization in a one-dimensional array of point Josephson junctions coupled to a common load, Phys. Rev. B **84**, 104501 (2011).

[33] R. A. Klemm, E. R. LaBerge, D. R. Morley, T. Kashiwagi, M. Tsujimoto, and K. Kadowaki, Cavity mode waves during terahertz radiation from rectangular $Bi_2Sr_2CaCu_2O_{8+\delta}$ mesas, J. Phys. Condens. Matter **23**, 025701 (2011).

[34] S. Lin and X. Hu, In-plane dissipation as a possible synchronization mechanism for terahertz radiation from intrinsic Josephson junctions of layered superconductors, Phys. Rev. B **86**, 054506 (2012).

[35] B. Gross, S. Guénon, J. Yuan, M. Y. Li, J. Li, A. Ishii, R. G. Mints, T. Hatano, P. H. Wu, D. Koelle, H. B. Wang, and R. Kleiner, Hot-spot formation in stacks of intrinsic Josephson junctions in $Bi_2Sr_2CaCu_2O_{8+\delta}$, Phys. Rev. B **86**, 094524 (2012).

[36] B. Gross, J. Yuan, D. Y. An, M. Y. Li, N. Kinev, X. J. Zhou, M. Ji, Y. Huang, T. Hatano, R. G. Mints, V. P. Koshelets, P. H. Wu, H. B. Wang, D. Koelle, and R. Kleiner, Modeling the linewidth dependence of coherent terahertz emission from intrinsic Josephson junction stacks in the hot-spot regime, Phys. Rev. B **88**, 014524 (2013).

[37] F. Liu, S. Lin, and X. Hu, Cavity phenomenon and terahertz radiation of a tall stack of intrinsic Josephson junctions wrapped by a dielectric material, Supercond. Sci. Technol. **26**, 025003 (2013).

[38] H. Asai and S. Kawabata, Intense terahertz emission from intrinsic Josephson junctions by external heat control, Appl. Phys. Lett. **104**, 112601 (2014).

[39] B. D. Josephson, Possible new effects in superconductive tunnelling, Phys. Lett. **1**, 251 (1962).

[40] K. Wiesenfeld, P. Colet, and S. H. Strogatz, Frequency locking in Josephson arrays: Connection with the Kuramoto model, Phys. Rev. E **57**, 1563 (1998).

[41] D. J. Watts and S. H. Strogatz, Collective dynamics of 'small-world' networks, Nature (London) **393**, 440 (1998).

[42] P. Kolodner and J. A. Tyson, Microscopic fluorescent imaging of surface temperature profiles with 0.01 °C resolution, Appl. Phys. Lett. **40**, 782 (1982).

[43] M. F. Crommie and A. Zettl, Thermal-conductivity anisotropy of single-crystal $Bi_2Sr_2CaCu_2O_8$, Phys. Rev. B **43**, 408 (1991).

[44] See http://www.comsol.com for details.